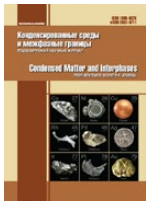

ISSN 1606-867X (Print)
ISSN 2687-0711 (Online)
Condensed Matter and Interphases
Kondensirovannye Sredy i Mezhfaznye Granitsy
https://journals.vsu.ru/kcmf/

Original articles

Research article
https://doi.org/10.17308/kcmf.2025.27/13020

Research on the influence of the powder stoichiometry of $(Ag_xCu_{1-x})_{0.7}GaSe_2$ on the phase composition, structure, and lifetime of photogenerated charge carriers

V. V. Rakitin[1]✉, M. V. Gapanovich[1,2,3], E. V. Rabenok[1], D. R. Kalimullina[2], D. S. Lutsenko[1,2], I. D. Kulemetev[2], E. N. Koltsov[1,3], A. V. Stanchik[4], V. F. Gremenok[4]

[1]Federal Research Center for Problems of Chemical Physics and Medicinal Chemistry, Russian Academy of Sciences, Academician Semenov av., 1, Chernogolovka, Moscow Region 142432, Russian Federation

[2]Lomonosov Moscow State University, Leninskiye Gory, 1, Moscow 119991, Russian Federation

[3]Moscow Center for Advanced Studies 20, Kulakova st., Moscow, Russian Federation

[2]Scientific-Practical Materials Research Centre, National Academy of Sciences of Belarus, 19 Petrusya Brovki st., Minsk 220072, Republic of Belarus

Abstract

Objective: This work presents a series of $(Ag_xCu_{1-x})_{0.7}GaSe_2$ ($0 \leqslant x \leqslant 1$) powders synthesized via a solid-state reaction using the presynthesized ternary compounds $Cu_{0.7}GaSe_2$, $Ag_{0.7}GaSe_2$, and $Ag_{0.7}GaSe_2$.

Experimental: A combination of X-ray diffraction (XRD) and Raman spectroscopy was used to establish that the solid solution region in this system is narrow and lies within the range of $0.8 \leqslant x < 1$.

Conclusions: An investigation of low-temperature luminescence spectra and microwave photoconductivity decay kinetics revealed that single-phase samples exhibit increased lifetimes of photogenerated charge carriers. This is attributed to the replacement of deep charge carrier traps, such as selenium vacancies V_{Se}, with shallower cationic copper vacancies associated with V_{Cu} and V_{Se}-V_{Cu}.

Keywords: Chalcopyrite powders, Copper quaternary compounds, Photoactive cathodes, Hydrogen generation

Funding: This work was financially supported by the Russian Science Foundation (RSF) (project number 24-43-10003) and the Belarusian Republican Foundation for Fundamental Research (project number Т23РНФМ-029). This research utilized a universal research facility "Unit for determining the lifetime of photogenerated current carriers by measuring microwave photoconductivity in the frequency range of 36 GHz" and equipment from the Analytical Center of the Federal Research Center for Problems of Chemical Physics and Medicinal Chemistry, RAS.

Acknowledgments: The authors thank Ph.D. D. V. Korchagin and Ph.D. (Phys.-Math.) G. F. Shilov for providing the XRD patterns; Ph.D. (Phys.-Math.) D. M. Sedlovets for providing the Raman spectra.

For citation: Rakitin V. V., Gapanovich M. V., Rabenok E. V., Kalimullina D. R., Lutsenko D. S., Kulemetev I. D., Koltsov E. N., Stanchik A. V., Gremenok V. F. Research on the influence of the powder stoichiometry of $(Ag_xCu_{1-x})_{0.7}GaSe_2$ on the phase composition, structure, and lifetime of photogenerated charge carriers. *Condensed Matter and Interphases*. 2025;27(3): 441–453. https://doi.org/10.17308/kcmf.2025.27/13020

Для цитирования: Ракитин В. В., Гапанович М. В., Рабенок Е. В., Калимуллина Д. Р., Луценко Д. С., Кулеметьев И. Д., Кольцов Е. Н., Станчик А. В., Гременок В. Ф. Исследование влияния стехиометрии порошков $(Ag_xCu_{1-x})_{0.7}GaSe_2$ на их фазовый состав, структуру и времена жизни фотогенерированных носителей тока. *Конденсированные среды и межфазные границы*. 2025;27(3): 441–453. https://doi.org/10.17308/kcmf.2025.27/13020

✉ Vladimir V. Rakitin, e-mail: domi-tyan@yandex.ru

1. Introduction

There is growing interest in the use of photoelectrochemical cells (PECs) for fuel production. It is known that light-driven water splitting into hydrogen and oxygen can occur on both photoactive anodes and cathodes [1]. The use of cathodes is considered a better solution because of their significantly lower degree of corrosion in PECs. III-V compound-based photoelectrodes are the most efficient for water splitting, but they are expensive and complex to manufacture [2]. Notably, for III-IV compounds, high efficiency is observed for photocathodes based on monocrystalline samples, whereas the efficiency drastically decreases for polycrystalline materials [3]. For complete light-driven water splitting in a PEC, the photocathode must possess an optimal bandgap (E_g) of ~1.7 eV but not less than 1.23 eV [1, 4]. Among suitable thin-film (1–2 μm) I-III-VI chalcopyrite semiconductors, $CuGaSe_2$ (E_g = 1.68 eV) and $AgGaSe_2$ (E_g = 1.8 eV) stand out [5].

The potential of using $AgGaSe_2$ – $CuGaSe_2$ solid solutions as photocathode materials was first described in [6]. It was established that photocathodes where a small amount of copper (~5%) is substituted with silver atoms yield higher photocurrents than do $CuGaSe_2$-based photocathodes. Furthermore, such materials do not degrade over extended periods, unlike CIGS-based photocathodes [6]. The viability of these materials for photocathodes has also been supported by studies [7, 8, 9]. The materials exhibit reasonably high photocurrent densities (18–27 mA/cm²) under AM 1.5 illumination. During PEC testing, no significant degradation was observed in the cathode region. A reduction occurs in the anode region, leading to the destruction of the film. For the p-CIGS/H2SO4 system, it should be noted that when the potential shifts to the negative region, the volume of released hydrogen increases (0.001 mL/cm² at –0.3 V and 0.009 mL/cm² at –0.6 V without illumination; 0.1 mL/cm² at –0.3 V and 1.5 mL/cm² at –0.6 V under illumination). Partial surface film degradation occurs during operation without significant chemical composition changes [5]. Voltammetric studies of the system yielded an open-circuit voltage V_{oc} = 0.663 V, short-circuit current density J_{sc} = 27.9 mA/cm², fill factor *FF* = 0.613, and efficiency η = 11.3% [6].

Several issues remain poorly explored. In particular, to increase the efficiency of CIGS-based solar cells, copper-deficient compounds must be used [10]. Furthermore, doping chalcopyrites with alkali metal ions significantly improves their efficiency [11]. However, this phenomenon has not been thoroughly investigated for photocathodes.

Thus, chalcopyrite-structured $AgGaSe_2$ – $CuGaSe_2$ solid solutions can be considered promising chemical materials for photocathodes in water splitting reactions for the production of hydrogen.

Specifically, [12] investigated the efficiency of solar light-driven water reduction on $CuGaSe_2$-based photocathodes with different monocrystalline plate orientations (321), (312), and (112). The results showed that after annealing in an Se atmosphere, copper-depleted compositions formed on the surface of plates with (321) and (312) orientations, whereas no copper depletion was observed on (112)-oriented plates. It is suggested that monocrystalline plates with copper-depleted compositions form a heterojunction that suppresses the recombination of photoexcited carriers. Compared with stoichiometric materials, photocathodes based on such plates are more efficient.

Reference [13] investigated the influence of the copper-to-gallium ratio on the crystal structure, morphology, and characteristics of Cu-Ga-Se film-based photocathodes obtained via one-step coevaporation. The authors showed that the surface morphology changes from large grains to fine columnar structures depending on the film composition. Different elemental ratios also affect the photocurrent density (j_{ph}) of the finished photocathode materials. To measure key photocathode characteristics, an electrochemical cell with a single *p-n* heterojunction, $Pt/CdS/CuGaSe_2$, was assembled from films with varying Cu/Ga ratios. The cell surface was modified with Pt particles atop the CdS layer. A 0.5 M H_2SO_4 electrolyte (pH = 0.4) and AM1.5 illumination were used. For films with Cu/Ga = 0.85, the photocurrent in this PEC was j_{ph} = 19.0 mA/cm², whereas for Cu/Ga = 0.33, the photocurrent decreased to

12.1 mA/cm² at –0.4 V. Conversely, at 0 V, for Cu/Ga = 0.85, the photocurrent was approximately 0 mA/cm², whereas for Cu/Ga = 0.33, it increased to 8.2 mA/cm². Other compositions, such as Cu/Ga = 1.17, 0.64, 0.44, 0.38, and 0.33, were also obtained in [13], but the near-stoichiometric composition (Cu/Ga = 1.17) was not investigated.

Since water splitting on photocathodes involves photogenerated electrons, one key factor influencing the efficiency of this process is the charge carrier lifetime. We previously established that partial substitution of copper with silver in $CuGaSe_2$ can increase these lifetimes [14]. Furthermore, in our work [15], for a series of $Ag_xCu_{1-x}GaSe_2$ solid solutions with x = 0, 0.3, 0.46, 0.63, and 1, it was found that the bandgap E_g changes nonlinearly: first decreasing and then increasing. Using a combination of low-temperature luminescence and time-resolved microwave photoconductivity (TRMC), it was shown that carrier lifetimes increase for samples with x values ranging from 0 to ~0.4 and again for those with x > 0.4. This phenomenon is due to the replacement of deep carrier traps, such as selenium vacancies, with shallower cationic vacancies.

Thus, investigating nonstoichiometric chalcopyrites as photoactive cathodes for photoelectrochemical water splitting is highly relevant. This work details the influence of the $(Ag_xCu_{1-x})_{0.7}GaSe_2$ powder stoichiometry on the phase composition, structure, and photogenerated charge carrier lifetime.

2. Experimental

$(Ag_xCu_{1-x})_{0.7}GaSe_2$ powder synthesis was carried out in two stages. First, the nonstoichiometric ternary chalcopyrite compounds $Cu_{0.7}GaSe_2$ and $Ag_{0.7}GaSe_2$ were prepared. The elemental copper, silver, gallium, and selenium were mixed at the required ratios, sealed in quartz ampoules under vacuum, and placed in a furnace at 1100 °C for 100 hours according to the following schemes:

$$0.7Cu + Ga + 2Se = Cu_{0.7}GaSe_2 \quad (1)$$

$$0.7Ag + Ga + 2Se = Ag_{0.7}GaSe_2 \quad (2)$$

After high-temperature synthesis, the products were extracted, ground into powder in an agate mortar, remixed in the required proportions, sealed in new quartz ampoules under vacuum, and annealed again at 650 °C for 100 hours. The proposed solid solution formation scheme is as follows:

$$x Ag_{0.7}GaSe_2 + (1-x)Cu_{0.7}GaSe_2 = (Ag_xCu_{1-x})_{0.7}GaSe_2 \quad (3)$$

This method minimizes component loss during synthesis.

The structure and phase composition of the $(Ag_xCu_{1-x})_{0.7}GaSe_2$ powders were studied via X-ray diffraction (XRD, PANalytical Aeris diffractometer, Cu-K_α radiation) and Raman spectroscopy (Bruker Senterra micro-Raman system, 532 nm excitation). Lattice parameters were determined via the WinXPoW(R) software package.

The defect structure was investigated by low-temperature luminescence at 78 K. Photoluminescence (PL) spectra were recorded via an MDR-23U monochromator in a custom optical cryostat. A Hamamatsu R9110 photomultiplier tube (200–850 nm range) was used at the monochromator exit slit. A 532 nm solid-state laser provided excitation.

Reflectance spectra were recorded on a Shimadzu UV-3101 PC spectrophotometer (300–2000 nm range, room temperature). The bandgap (E_g) was determined by replotting optical spectra in $[h\nu - Y(h\nu)]^2$ vs. $h\nu$ coordinates for direct bandgap semiconductors. The absorption coefficient was estimated via the Kubelka–Munk equation:

$$Y(h\nu) = \frac{(1-R)^2}{2R} \sim \alpha \quad (4)$$

where R is the reflectance and α is the absorption coefficient.

The kinetics of photogenerated carrier decay were studied in a contact-free manner via time-resolved microwave photoconductivity at 36 GHz (Universal Research Facility "Unit for determining the lifetime of photogenerated current carriers by measuring microwave photoconductivity in the frequency range of 36 GHz") [16]. The photoconductivity was excited by an LGI 505 nitrogen laser (λ = 337 nm, t_{pulse} = 8 ns). The detection circuit temporal resolution was ~5 ns. The maximum incident light flux density was 10^{16} photons/cm² per pulse. The light intensity was varied via filters.

3. Results and discussion

3.1. XRD data

Fig. 1a shows the XRD patterns of the $(Ag_xCu_{1-x})_{0.7}GaSe_2$ powders at $0 \leqslant x \leqslant 1$. A decreasing silver content shifted the main peaks toward higher angles, particularly for the most intense (112), (220)/(204), and (312)/(116) lines.

On the basis of Figs. 1b and 1c, only the end-member $Cu_{0.7}GaSe_2$ and solid solution powder $(Ag_xCu_{1-x})_{0.7}GaSe_2$ in the range $0.8 \leqslant x < 1$ are single-phase. Powders with compositions in the $0.7 \leqslant x \leqslant 0.1$ range are multiphase.

Fig. 2 shows diffractograms of the end-member powders $Cu_{0.7}GaSe_2$ (a) and $Ag_{0.7}GaSe_2$ compared with the stoichiometric $CuGaSe_2$ and $AgGaSe_2$ obtained previously in [15].

Fig. 2a shows that the peak positions for nonstoichiometric $Cu_{0.7}GaSe_2$ are slightly shifted relative to those of stoichiometric $CuGaSe_2$. No impurity phases were detected; the structure remained tetragonal with space group *I*-42*d* [17, 18, 19, 20]. Fig. 2b shows that the peak positions for nonstoichiometric $Ag_{0.7}GaSe_2$ and stoichiometric $AgGaSe_2$ coincide completely. However, the diffractogram of $Ag_{0.7}GaSe_2$ exhibits additional lines (marked *) corresponding to the cubic Ga_2Se_3 phase (space group *F*-43 m) [21, 22]. Table 1 lists the lattice parameter a and unit cell volume *V* values for single-phase end-member $Cu_{0.7}GaSe_2$ and solid solution powders $(Ag_xCu_{1-x})_{0.7}GaSe_2$ in the range $0.8 \leqslant x < 1$.

This observation can be explained by considering $Cu_{0.7}GaSe_2$ as a solid solution of $Cu^{I}GaSe_2$ – $Cu^{II}Ga_2Se_4$. Silver, however, does not typically exhibit Ag^{II} valence. Therefore, increasing δ in $Ag_{1-\delta}GaSe_2$ leads to decomposition according to Scheme (5):

$$Ag_{0.7}GaSe_2 \rightarrow 0.7\ AgGaSe_2 + 0.15Ga_2Se_3 + 0.15Se \quad (5)$$

Annealing $Cu_{0.7}GaSe_2$ with $Ag_{0.7}GaSe_2$ powders may induce a disproportionation reaction (6):

$$x\,Ag_{0.7}GaSe_2 + (1-x)Cu_{0.7}GaSe_2 = 0.7x\,AgGaSe_2 + (1-0.7x)Cu_{\frac{0.7-0.7x}{1-0.7x}}GaSe_2. \quad (6)$$

According to this reaction, some copper undergoes a transition from Cu^{I} to Cu^{II}. The single-phase region depends on *x*, governed by the mutual solubility of the resulting components, and the maximum possible deviation from the copper stoichiometry in $Cu_{1-\delta}GaSe_2$: *1*-δ cannot be less than 0.5, as all copper Cu^{I} would transition to Cu^{II}. This explains the initial disappearance of the Ga_2Se_3 phase in the XRD patterns of the synthesized $(Ag_xCu_{1-x})_{0.7}GaSe_2$ samples within $0.8 \leqslant x < 1$ and its reappearance at higher *x* values.

Fig. 3 shows the lattice parameters and unit cell volume *V* for single-phase $(Ag_xCu_{1-x})_{0.7}GaSe_2$ samples as a function of *x*.

For samples with *x* values ranging from 1 to 0.7, the lattice parameters change linearly, and the unit cell volume increases. This indicates the formation of solid solutions based on $AgGaSe_2$ for these *x* and δ values.

3.2. Raman spectroscopy data

Fig. 4 shows the Raman spectra of nonstoichiometric $(Ag_xCu_{1-x})_{0.7}GaSe_2$ powders with varying copper and silver contents. All the spectra confirm the presence of chemical bonds in the $(Ag_xCu_{1-x})_{0.7}GaSe_2$ compounds for different values of *x*. The main peak shifts toward higher energies when the peak transitions from the $x = 1$ end-member (177 cm^{-1}) to the $x = 0$ end-member (184 cm^{-1}), which is consistent with our previous findings for stoichiometric $Ag_xCu_{1-x}GaSe_2$ powders [15].

Fig. 5 shows the Raman spectra for the end-member powders $Cu_{0.7}GaSe_2$ and $Ag_{0.7}GaSe_2$

Table 1. Values of bandgap E_g, lattice parameter *a*, and unit cell volume *V* for $(Ag_xCu_{1-x})_{0.7}GaSe_2$ powders

Samples	E_g, eV	E_g, theoret. [24]	*a*, Å	*V*, Å^3
$Cu_{0.7}GaSe_2$	1.65	1.77	5.5863(28)	343.18(16)
$(Ag_{0.8}Cu_{0.2})_{0.7}GaSe_2$	1.68	1.76	5.9250(22)	379.00(15)
$(Ag_{0.9}Cu_{0.1})_{0.7}GaSe_2$	1.71	1.75	5.9500(23)	378.01(16)
$AgGaSe_2$ [15]	1.76	1.82	5.9895(30)	390.25(15)

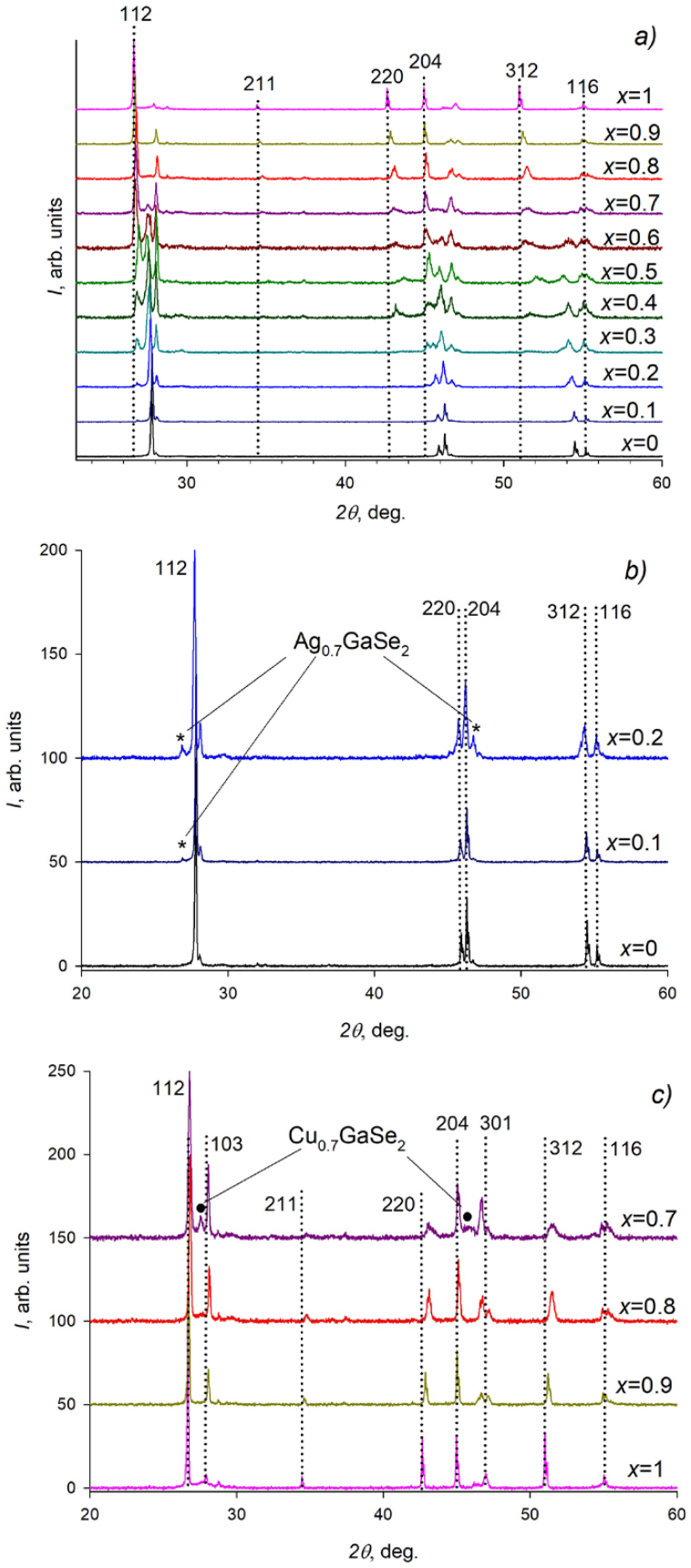

Fig. 1. XRD patterns of $(Ag_xCu_{1-x})_{0.7}GaSe_2$ powders for $0 \leqslant x \leqslant 1$ (a), $0 \leqslant x \leqslant 0.2$ (b) and $0.7 \leqslant x \leqslant 1$ (c)

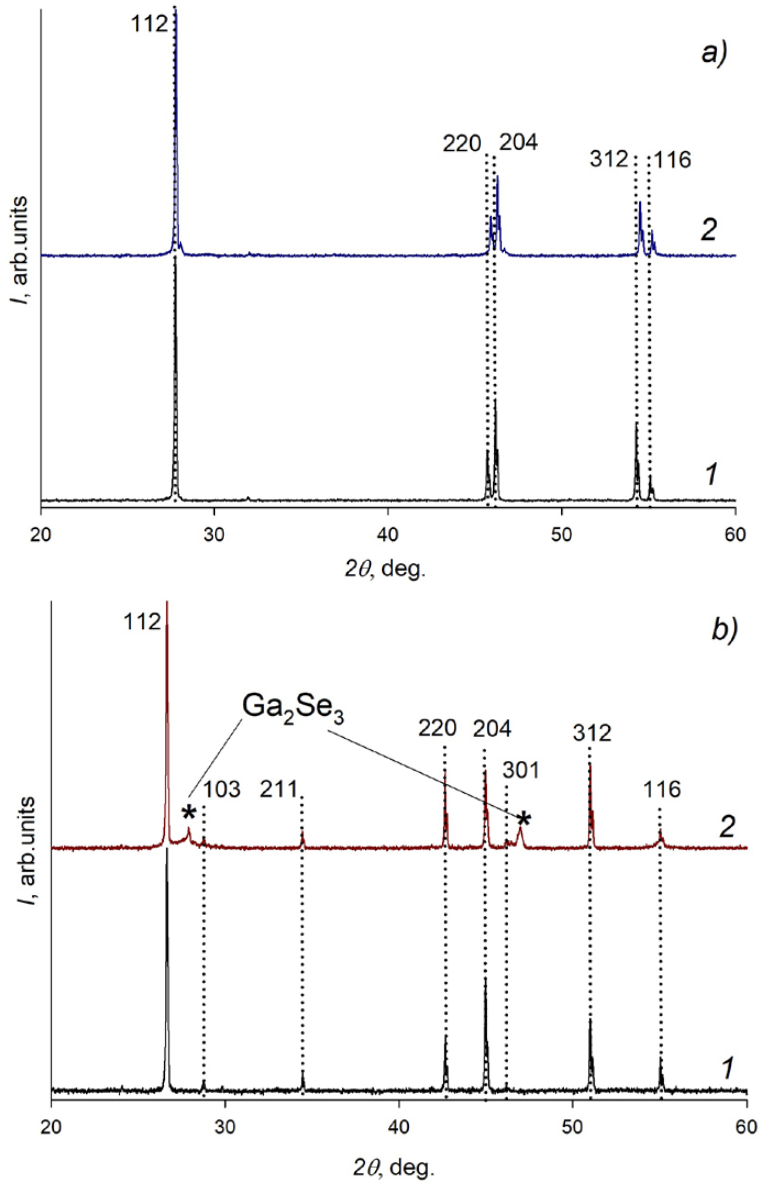

Fig. 2. XRD patterns for end-member powders: (a) Powders with copper content: $CuGaSe_2$ [15] (*1*) and $Cu_{0.7}GaSe_2$ (*2*); (b) Powders with silver content: $AgGaSe_2$ [15] (*1*) and $Ag_{0.7}GaSe_2$ (*2*)

compared with the stoichiometric $CuGaSe_2$ and $AgGaSe_2$ obtained in [15]. The peak positions for nonstoichiometric powders at x = 0 and x = 1 agree well with the literature data [23, 24] for stoichiometric $CuGaSe_2$ and $AgGaSe_2$ chalcopyrites.

The peaks at 184 cm^{-1} (Fig. 5a) and 177 cm^{-1} (Fig. 5b), for stoichiometric compositions, belong to the A_1 mode, attributed to vibrations of the Se atom relative to stationary Cu or Ag atoms. As shown in [15], other peaks at approximately 246, 252, and 273 cm^{-1} belong to various B_2 modes, primarily involving vibrations of Ga cations relative to the Se atom. Their positions change less noticeably with powder composition: at x = 1, peaks at 252 cm^{-1} dominate, whereas at x = 0, peaks at 246 and 273 cm^{-1} become more intense.

However, in Fig. 5b for $Ag_{0.7}GaSe_2$ (*curve 2*), an additional peak at 287 cm^{-1} is observed, along with less intense lines (marked *). Their appearance can be explained by the formation of the Ga_2Se_3 phase and amorphous Se according to Scheme (5), as corroborated by the XRD data.

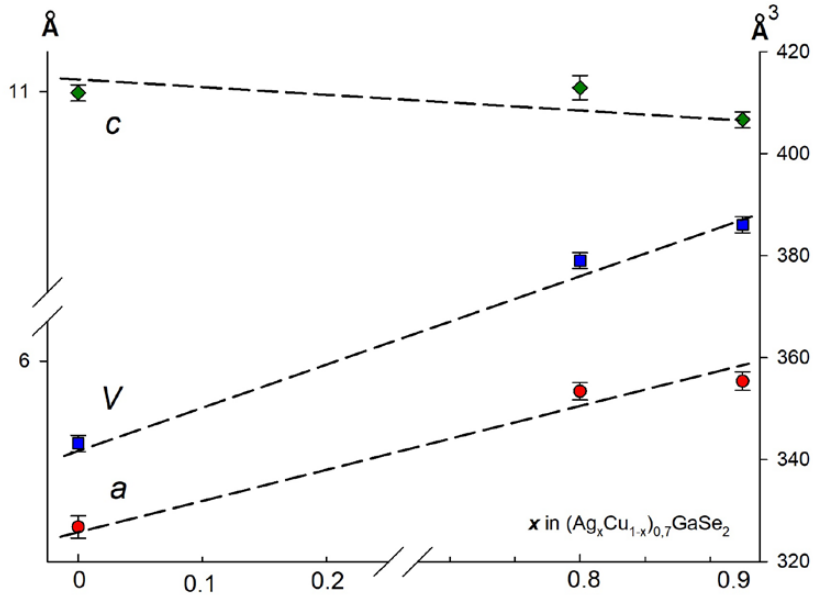

Fig. 3. Dependence of the lattice parameters *a* and c and the unit cell volume *V* on the composition of the $(Ag_xCu_{1-x})_{0.7}GaSe_2$ powders

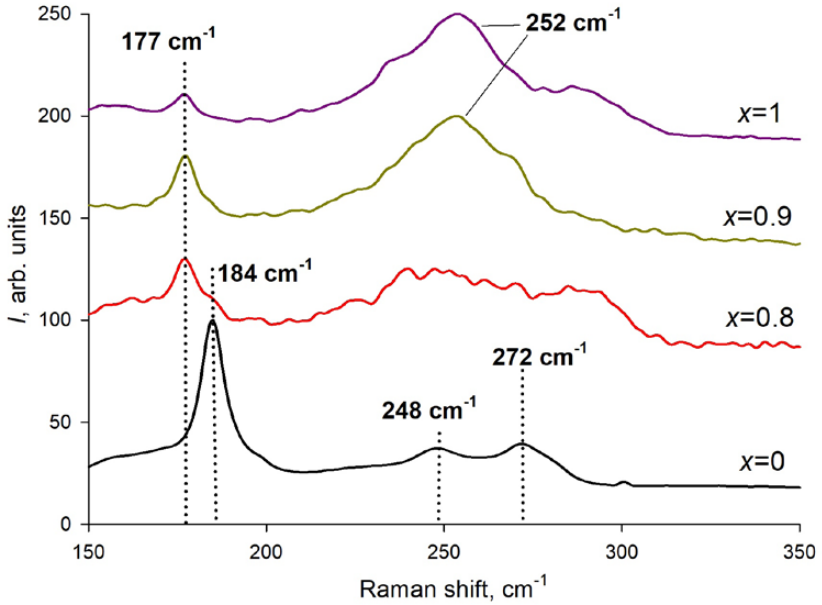

Fig. 4. Raman spectra of the $(Ag_xCu_{1-x})_{0.7}GaSe_2$ powders

3.3. Bandgap determination in powders

Fig. 6 shows absorption spectra plotted as $[h\nu–Y(h\nu)]^2$ vs. $h\nu$, derived via the Kubelka–Munk formula.

As shown in Fig. 6a, the bandgap for the $Cu_{0.7}GaSe_2$ powder is ~1.69 eV, which is slightly greater than that for the $CuGaSe_2$ powder [15]. This is explained by $Cu_{0.7}GaSe_2$ being a solid solution of $Cu^{I}GaSe_2$ – $Cu^{II}Ga_2Se_4$. For single-phase $(Ag_xCu_{1-x})_{1-\delta}GaSe_2$ samples, the bandgap decreases smoothly from 1.76 eV to 1.68 eV when $AgGaSe_2$ [15] transitions to $(Ag_{0.8}Cu_{0.2})_{0.7}GaSe_2$.

Table 1 lists the bandgap E_g, lattice parameter *a*, and unit cell volume *V* values for the $(Ag_xCu_{1-x})_{0.7}GaSe_2$ powders. Theoretical E_g values from [25] are included for comparison. The

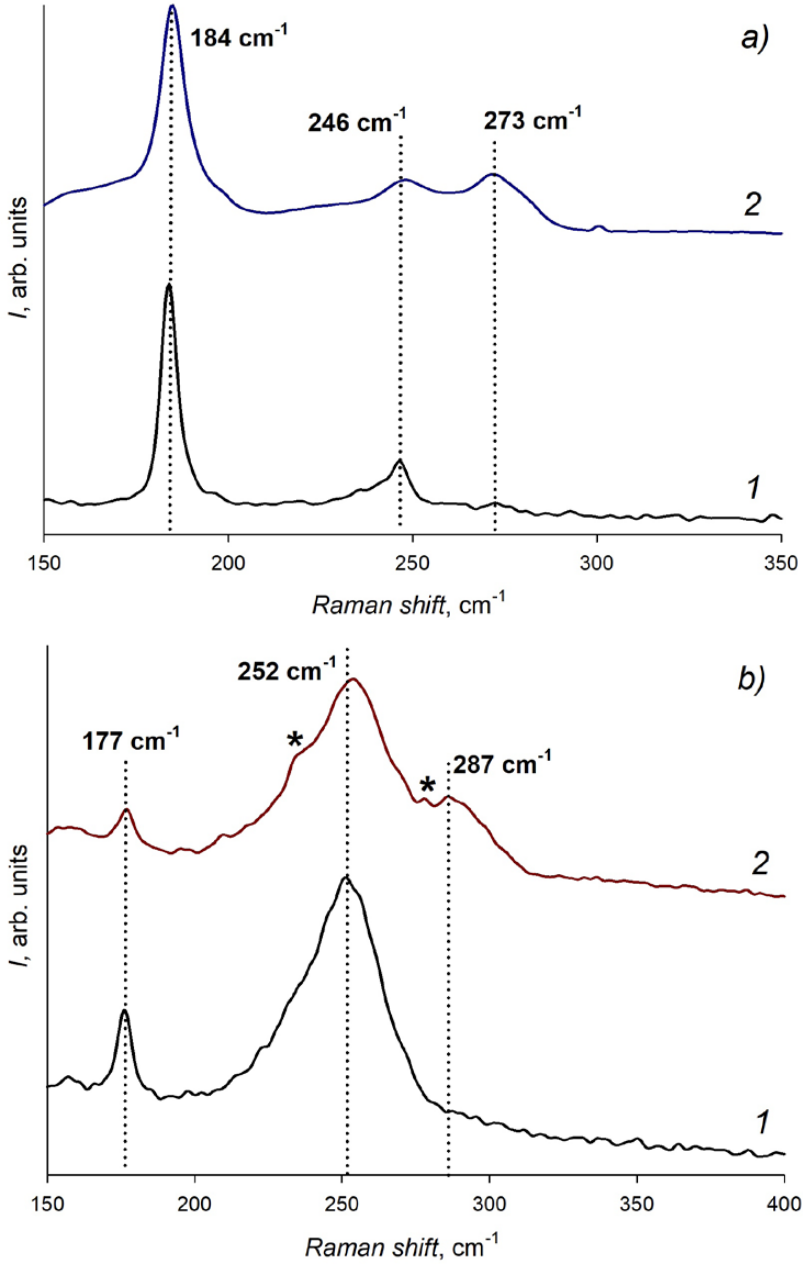

Fig. 5. Raman spectra of end-member powders: (a) Powders with copper content: $CuGaSe_2$ [15] (*1*) and $Cu_{0.7}GaSe_2$ (*2*); (b) Powders with silver content: $AgGaSe_2$ [15] (*1*) and $Ag_{0.7}GaSe_2$ (*2*)

theoretical values calculated in [25] are somewhat higher than our experimental values for analogous compositions. However, both the theoretical and experimental E_g values increase with increasing x in $(Ag_xCu_{1-x})_{1-\delta}GaSe_2$. The smooth bandgap variation for these compositions can be explained by the increasing unit cell volume. A similar trend, but over a wider x range, was observed for stoichiometric $Ag_xCu_{1-x}GaSe_2$ powders in our previous work [15].

3.4. Low temperature luminescence spectra

Fig. 7 shows smoothed, normalized low-temperature luminescence spectra (78 K) for AgGaSe2 [15] (Fig. 7a), Cu0.7GaSe2 (Fig. 7d), and solid solutions based on them with various silver contents (Fig. 7b, c). The spectra exhibit a significant full width at half maximum (FWHM) and are probably composite. Deconvolution into multiple Lorentzian curves revealed the peak maxima. The deconvolution results and

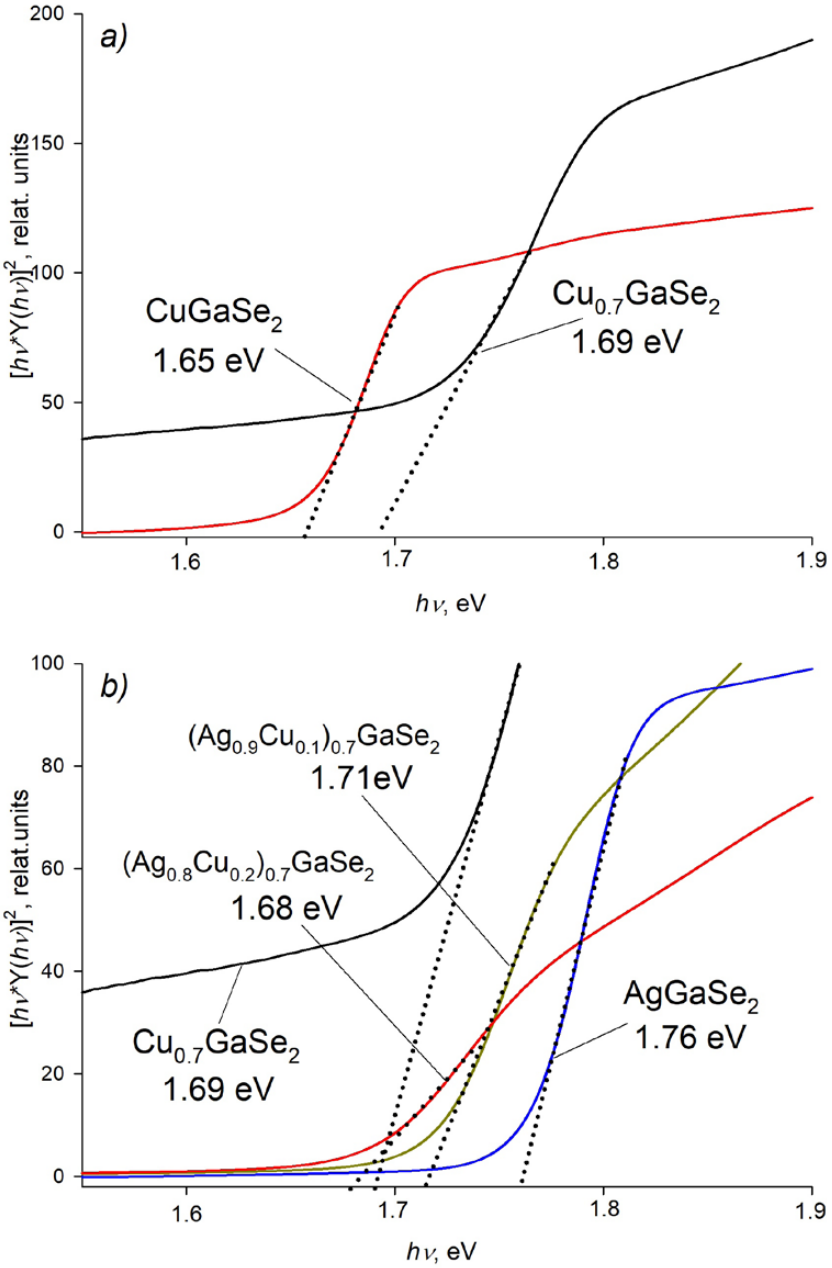

Fig. 6. Determination of E_g in $[h\nu - Y(h\nu)]^2$ vs. $h\nu$ coordinates for $Cu_{1-x}GaSe_2$ (a) and $(Ag_xCu_{1-x})_{0.7}GaSe_2$ powders (*b*)

experimental E_g values are listed in Table 2. All the spectra, except those for $CuGaSe_2$ and $AgGaSe_2$, can be decomposed into 3 peaks, denoted E_1, E_2, and E_3 in the table. Minor differences in their maxima are due to the varying E_g values of the samples. On the basis of the room-temperature bandgap values, the first peak E_1 corresponds to a deep acceptor level, E_2 corresponds to a shallower level (likely a donor), and E_3 corresponds to a shallow donor level or band-to-band transition.

The slightly higher energy of the E_3 peak than that of the *Eg* peak at room temperature is due to the temperature-induced increase in the semiconductor E_g upon cooling. For example, according to [26], $AgGaSe_2$ has an E_g = 1.824 eV at 4 K. It can be assumed that the E_3 peak arises from a shallow donor level rather than a band-to-band transition. According to [27], low-temperature (4 K) spectra of $AgGaSe_2$ show peaks at E = 1.724 eV (attributed to selenium vacancies V_{Se}) and

E = 1.764 eV (attributed to cationic vacancies V_{cat}). The authors studied undoped $CuGaSe_2$ powders by low-temperature luminescence at 10 K [28] and reported predominant emission at E = 1.67 eV, which is consistent with [29] and explained by copper vacancy formation. Thus, for the $Cu_{0.7}GaSe_2$, $(Ag_{0.8}Cu_{0.2})_{0.7}GaSe_2$ and $(Ag_{0.9}Cu_{0.1})_{0.7}GaSe_2$ samples, the E_3 peak may be attributed to this specific defect. Furthermore, for the $(Ag_xCu_{1-x})_{0.7}GaSe_2$ samples with $0.8 \leqslant x < 1$, a slight increase in the E_3 peak intensity is observed, which is explained by a decrease in the copper content and a consequent increase in the V_{Cu} concentration according to Scheme (6).

The E_2 peak for $AgGaSe_2$ may originate from V_{Se}–V_{Cu} defect associations, which form shallower levels than isolated selenium vacancies (V_{Se}). Thus, for the $(Ag_{0.8}Cu_{0.2})_{0.7}GaSe_2$ and $(Ag_{0.9}Cu_{0.1})_{0.7}GaSe_2$ samples, the deep acceptor levels (V_{Se}) are partially replaced by shallower donor levels, where V_{Cu} and V_{Se}-V_{Cu} are associated.

3.5. Photogenerated charge carrier lifetime data

An investigation of the photogenerated carrier decay kinetics in $(Ag_xCu_{1-x})_{0.7}GaSe_2$ powders revealed that the measured microwave photoconductivity decays are well approximated by either a single exponential or the sum of two exponential functions: “fast” and “slow” (Fig. 8). Table 3 lists the characteristic decay times of the fast τ_f and slow τ_s components of the microwave photoresponse. Biphasic kinetics are characteristic of only the $(Ag_{0.9}Cu_{0.1})_{0.7}GaSe_2$ sample. The presence of a slow component indicates processes related to the thermal release of carriers from traps and depends on trap depth. As shown by the low-temperature luminescence

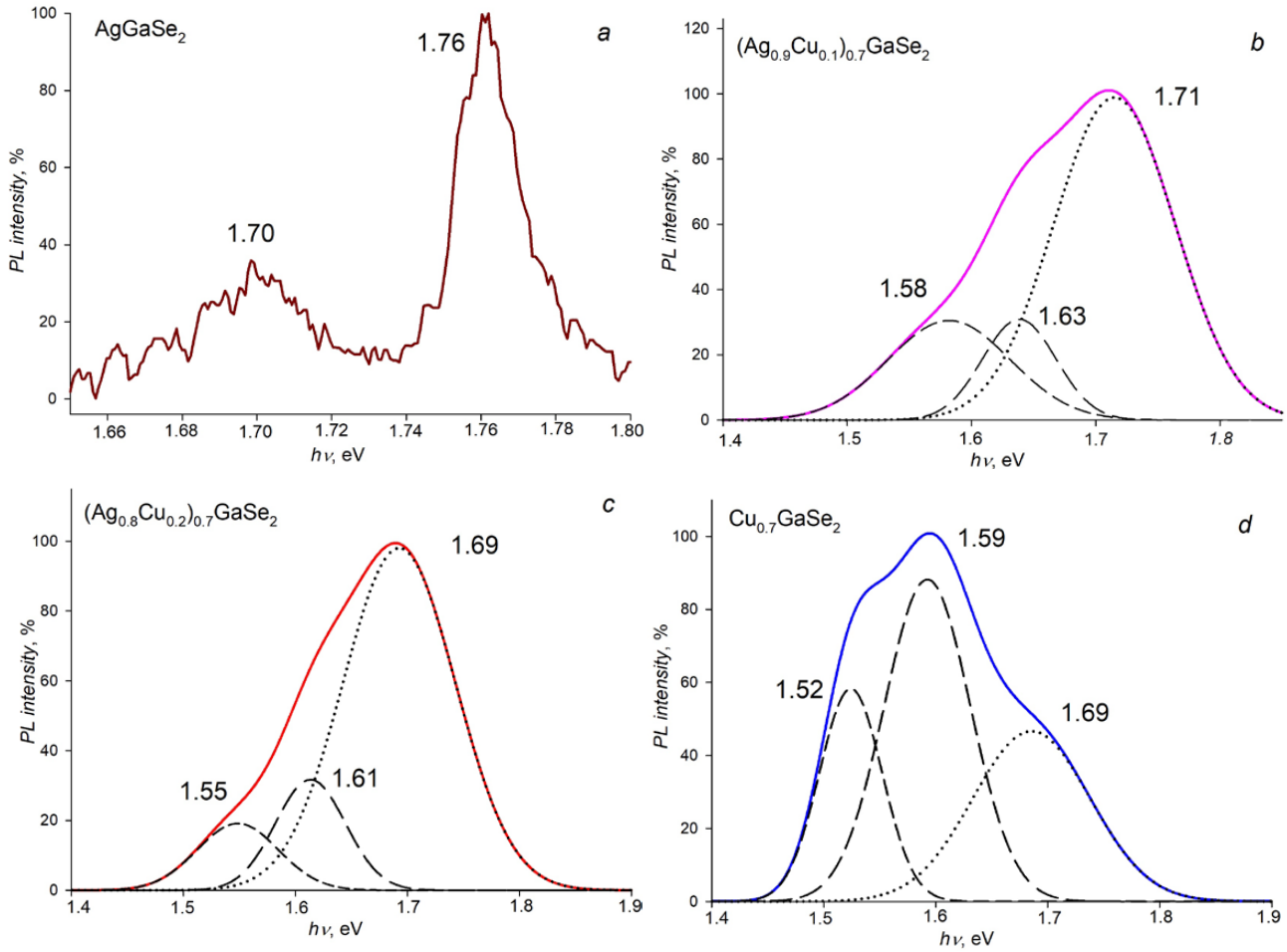

Fig. 7. Low-temperature luminescence spectra (T = 78 K) for $AgGaSe_2$ [15] (a), $(Ag_{0.9}Cu_{0.1})_{0.7}GaSe_2$ (b), $(Ag_{0.8}Cu_{0.2})_{0.7}GaSe_2$ (c), and $Cu_{0.7}GaSe_2$ (d) powders

Table 2. Maximum E_1, E_2, and E_3 values in low-temperature luminescence spectra (78 K) and experimental E_g values for $(Ag_xCu_{1-x})_{0.7}GaSe_2$ powders

Samples	E_1, eV	I, %	E_2, eV	I, %	E_3, eV	I, %	E_g, eV
$CuGaSe_2$ [15]	–	-	**–**	-	**1.63**	100	**1.65**
$Cu_{0.7}GaSe_2$	**1.52**	67	**1.59**	100	**1.69**	67	**1.65**
$(Ag_{0.8}Cu_{0.2})_{0.7}GaSe_2$	**1.55**	19	**1.61**	31	**1.69**	100	**1.68**
$(Ag_{0.9}Cu_{0.1})_{0.7}GaSe_2$	**1.58**	31	**1.63**	31	**1.71**	100	**1.71**
$AgGaSe_2$ [15]	**1.70**	32	–	–	**1.76**	100	**1.76**

spectra, the compositions $(Ag_{0.8}Cu_{0.1})_{0.7}GaSe_2$ and $(Ag_{0.9}Cu_{0.1})_{0.7}GaSe_2$ exhibit partial replacement of deep acceptor levels (V_{Se}) with shallower donor levels, which are associated with V_{Cu} and V_{Se}–V_{Cu}. Thus, it can be assumed that for $(Ag_{0.7}Cu_{0.1})_{0.7}GaSe_2$, selenium vacancies ($V_{Se}$), which act as deep acceptor traps, are the predominant defects. Upon transitioning to the $(Ag_{0.9}Cu_{0.1})_{0.7}GaSe_2$ composition, shallower traps, i.e., copper vacancies (V_{Cu}) and vacancies associated with V_{Se}–V_{Cu}, which act as shallow acceptor traps, become dominant.

4. Conclusion

A series of samples with the general formula $(Ag_xCu_{1-x})_{0.7}GaSe_2$ ($0 \leqslant x \leqslant 1$) were synthesized via a solid-state reaction. The solid solution region in this system is narrower than that in previously studied $Ag_xCu_{1-x}GaSe_2$ and lies within $0.8 \leqslant x < 1$. The structure of the samples is tetragonal (space group I-42d). The narrower x range is likely caused by a disproportionation reaction:

$$x\,Ag_{0.7}GaSe_2 + (1-x)Cu_{0.7}GaSe_2 =$$
$$= 0.7x\,AgGaSe_2 = (1-0.7x)Cu_{\frac{0.7-0.7x}{1-0.7x}}GaSe_2.$$

Using a combination of low-temperature luminescence and time-resolved microwave photoconductivity, it was shown that carrier lifetimes increase for sample series with $x = 0$ and $0.8 \leqslant x < 1$. This phenomenon appears to be caused by the replacement of deep charge carrier traps, such as selenium vacancies (V_{Se}), with shallower cationic copper vacancies associated with V_{Cu} and V_{Se}–V_{Cu}.

Contribution of the authors

The authors contributed equally to this article.

Conflict of interests

The authors declare that they have no known competing financial interests or personal relationships that could have influenced the work reported in this paper.

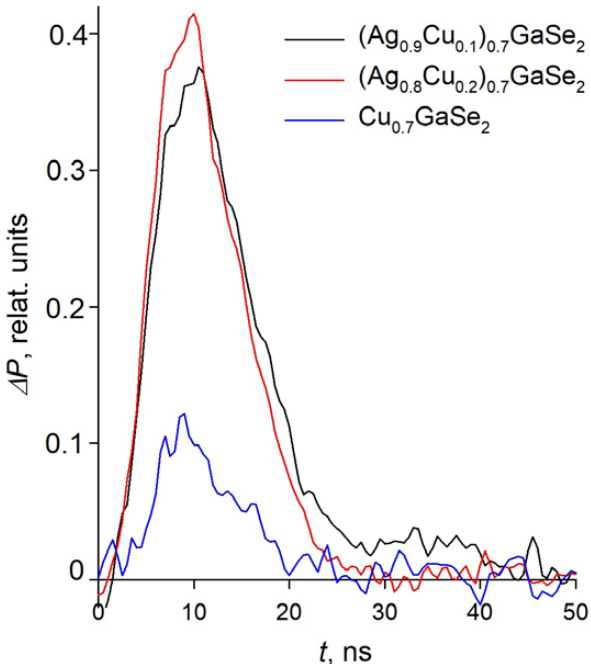

Fig. 8. The microwave photoconductivity decays for the $(Ag_{0.9}Cu_{0.1})_{0.7}GaSe_2$, $(Ag_{0.8}Cu_{0.2})_{0.7}GaSe_2$ and $Cu_{0.7}GaSe_2$ powders. $I = 10^{16}$ photons/cm^2 per pulse

Table 3. Characteristic decay times of the fast, τ_f, and slow, τ_s, components of the microwave photoresponse

Samples	$\tau_б$, ns	$\tau_м$, ns
$Cu_{0.7}GaSe_2$	5	–
$(Ag_{0.8}Cu_{0.2})_{0.7}GaSe_2$	5	–
$(Ag_{0.9}Cu_{0.1})_{0.7}GaSe_2$	5	100
$AgGaSe_2$ [15]	12	910

References

1. Turner J. A. Sustainable hydrogen production. *Science*. 2004;305(5686): 972-4. https://doi.org/10.1126/science.1103197

2. Chiu Y. H., Lai T. H., Kuo M. Y., Hsieh P. Y., Hsu Y. J. Photoelectrochemical cells for solar hydrogen production: Challenges and opportunities. *APL Materials*. 2019;7(8). https://doi.org/10.1063/1.5109785

3. Yokoyama D., Minegishi T., Maeda K., ... Domen K. Photoelectrochemical water splitting using a Cu(In, Ga)Se_2 thin film. *Electrochemistry Communications*. 2010;12(6): 851–853. https://doi.org/10.1016/j.elecom.2010.04.004

4. Barreto L., Makihira A., Riahi K. The hydrogen economy in the 21st century: a sustainable development scenario. *International Journal of Hydrogen Energy*. 2003;28(3): 267–284. https://doi.org/10.1016/S0360-3199(02)00074-5

5. Chen Y., Feng X., Liu M., Su J., Shen S. Towards efficient solar-to-hydrogen conversion: fundamentals and recent progress in copper-based chalcogenide photocathodes. *Nanophotonics*. 2016;5(4): 524–547. https://doi.org/10.1515/nanoph-2016-0027

6. Zhang L., Minegishi T., Kubota J., Domen K. Hydrogen evolution from water using $Ag_xCu_{1-x}GaSe_2$ photocathodes under visible light. *Physical Chemistry Chemical Physics*. 2014;16(13): 6167–6174. https://doi.org/10.1039/c3cp54590c

7. Valderrama R. C., Sebastian P. J., Enriquez J. P., Gamboa S. A. Photoelectrochemical characterization of CIGS thin films for hydrogen production. *Solar Energy Materials and Solar Cells*. 2005;88(2): 145–155. https://doi.org/10.1016/j.solmat.2004.10.011

8. Marsen B., Dorn S., Cole B., Rocheleau R. E., Miller E. L. Copper chalcopyrite film photocathodes for direct solar-powered water splitting. *MRS Online Proceedings Library (OPL)*. 2006;974: 0974-CC09. https://doi.org/10.1557/PROC-0974-CC09-05

9. Jacobsson T. J., Platzer-Björkman C., Edoff M., Edvinsson T. $CuIn_xGa_{1-x}Se_2$ as an efficient photocathode for solar hydrogen generation. *International Journal of Hydrogen Energy*. 2013;38(35): 15027–15035. https://doi.org/10.1016/j.ijhydene.2013.09.094

10. Conibeer G., Willoughby A. (eds.). *Solar cell materials: developing technologies*. John Wiley & Sons; 2014. 344 p. https://doi.org/10.1002/9781118695784

11. Rudmann D., Brémaud D., Zogg H., Tiwari A. N. Na incorporation into Cu(In, Ga)Se_2 for high-efficiency flexible solar cells on polymer foils. *Journal of Applied Physics*. 2005;97(8). https://doi.org/10.1063/1.1857059

12. Ikeda S., Fujita W., Katsube R., ... Yoshino K. Crystalline-face-dependent photoelectrochemical properties of single crystalline $CuGaSe_2$ photocathodes for hydrogen evolution under sunlight radiation. *Electrochimica Acta*. 2023;454: 142384. https://doi.org/10.1016/j.electacta.2023.142384

13. Mahmoudi B., Caddeo F., Lindenberg T., ... Maijenburg A. W. Photoelectrochemical properties of Cu-Ga-Se photocathodes with compositions ranging from $CuGaSe_2$ to $CuGa_3Se_5$. *Electrochimica Acta*. 2021;367: 137183. https://doi.org/10.1016/j.electacta.2020.137183

14. Rabenok E. V., Gapanovich M. V. Study of the decay kinetics of photogenerated current carriers in $Ag_{1-x}Cu_xGaSe_2$ solid solutions. *High Energy Chemistry*. 2023;57(2): 174–175. https://doi.org/10.1134/S0018143923020108

15. Rakitin V. V., Gapanovich M. V., Lutsenko D. S., ... Kabyliatski A. V. Studying the effect of composition on the crystal structure, optical properties, and photogenerated current carriers lifetimes in $Ag_xCu_{1-x}GaSe_2$ ($0 \leqslant x \leqslant 1$) solid solutions. *High Energy Chemistry*. 2024;58(5): 492-498. https://doi.org/10.1134/S0018143924700474

16. Novikov G. F., Marinin A. A., Rabenok E. V. Microwave measurements of the pulsed photoconductivity and photoelectric effect. *Instruments and Experimental Techniques*. 2010;53(2): 233–239. https://doi.org/10.1134/S0020441210020144

17. Barman B., Handique K. C., Kalita P. K. Observation of negative differential resistance (NDR) in chemically synthesized $CuGaSe_2$ nanorods. *Materials Letters*. 2024;357: 135638. https://doi.org/10.1016/j.matlet.2023.135638

18. Swamy H. G., Naidu B. S., Reddy P.J. Structure and optical properties of $CuGaSe_2$ thin films. *Vacuum*. 1990; 41(4-6): 1445–1447. https://doi.org/10.1016/0042-207X(90)93985-R

19. Karaagac H., Parlak M. Effects of annealing on structural and morphological properties of e-beam evaporated $AgGaSe_2$ thin films. *Applied Surface Science*. 2009;255(11): 5999–6006. https://doi.org/10.1016/j.apsusc.2009.01.054

20. Karaagac H., Parlak M. Deposition and characterization of layer-by-layer sputtered $AgGaSe_2$ thin films. *Applied Surface Science*. 2011;257(13): 5731–5738. https://doi.org/10.1016/j.apsusc.2011.01.087

21. Isik M., Gasanly N. M. Investigation of structural and optical characteristics of thermally evaporated Ga_2Se_3 thin films. *Vacuum*. 2020;179: 109501. https://doi.org/10.1016/j.vacuum.2020.109501

22. Isik M., Sarigul N., Gasanly N. M. Thermoluminescence characteristics of GaSe and Ga2Se3 single crystals. *Journal of Luminescence*. 2022;246: 118846. https://doi.org/10.1016/j.jlumin.2022.118846

23. Theodoropoulou S., Papadimitriou D., Doka S., Schedel-Niedrig T., Lux-Steiner M. C. Structural properties of Ge doped $CuGaSe_2$ films studied by Raman and photoluminescence spectroscopy. *Thin Solid Films*. 2007; 515(15): 5904–5908. https://doi.org/10.1016/j.tsf.2006.12.163

24. Cui Y., Roy U. N., Bhattacharya P., Parker A., Burger A., Goldstein J. T. Raman spectroscopy study of $AgGaSe_2$, $AgGa_{0.9}In_{0.1}Se_2$, and $AgGa_{0.8}In_{0.2}Se_2$ crystals. *Solid State Communications*. 2010;150(35-36): 1686–1689. https://doi.org/10.1016/j.ssc.2010.06.022

25. Boyle J. H., McCandless B. E., Shafarman W. N., Birkmire R. W. Structural and optical properties of (Ag, Cu)(In, Ga)Se_2 polycrystalline thin film alloys. *Journal of Applied Physics*. 201;115(22). https://doi.org/10.1063/1.4880243

26. Nigge K. M., Baumgartner F. P., Bucher E. CVT-growth of $AgGaSe_2$ single crystals: electrical and photoluminescence properties. *Solar Energy Materials and Solar Cells*. 1996;43(4): 335–343. https://doi.org/10.1016/0927-0248(96)00007-4

27. Artus L., Bertrand Y. Anomalous temperature dependence of fundamental gap of $AgGaS_2$ and $AgGaSe_2$ chalcopyrite compounds. *Solid State Communications*. 1987;61(11): 733–736. https://doi.org/10.1016/0038-1098(87)90727-7

28. Weiss T., Birkholz M., Saad M., ... Lux-Steiner M. C. Ag-doped $CuGaSe_2$ as a precursor for thin film solar cells. *Journal of Crystal Growth*. 1999;198: 1190–1195. https://doi.org/10.1016/S0022-0248(98)01152-X

29. Schön J. H., Riazi-Nejad H., Kloc C., Baumgartner F. P., Bucher E. Photoluminescence properties of doped-and undoped-$CuGaSe_2$ single crystals. *Journal of Luminescence*. 1997;72: 118–120. https://doi.org/10.1016/S0022-2313(96)00385-7

Information about the authors

Vladimir V. Rakitin, Cand. Sci. (Chem.), Senior Researcher, Group of Semiconductor and Composite Materials, Federal Research Center for Problems of Chemical Physics and Medicinal Chemistry, RAS (Chernogolovka, Moscow Region, Russian Federation).
https://orcid.org/0000-0001-6582-5212
domi-tyan@yandex.ru

Mikhail V. Gapanovich, Cand. Sci. (Chem.), Head of Group, Group of Semiconductor and Composite Materials, Federal Research Center for Problems of Chemical Physics and Medicinal Chemistry, RAS (Chernogolovka, Moscow Region, Russian Federation).
https://orcid.org/0000-0002-9109-6532
gmw1@mail.ru

Evgenia V. Rabenok, Cand. Sci. (Phys.-Math.), Senior Researcher, Group of Semiconductor and Composite Materials, Federal Research Center for Problems of Chemical Physics and Medicinal Chemistry, RAS (Chernogolovka, Moscow Region, Russian Federation).
https://orcid.org/0000-0002-3500-6918
jane.rabenok@yandex.ru

Dana R. Kalimullina, 6th year student, Faculty of Physics, Lomonosov Moscow State University (Moscow, Russian Federation).
kalimullinadana@mail.ru

Denis S. Lutsenko, Junior Researcher, Group of Semiconductor and Composite Materials, Federal Research Center for Problems of Chemical Physics and Medicinal Chemistry, RAS (Moscow, Russian Federation).
lutsenkods@my.msu.ru

Ivan D. Kulemetev, 5th year student, Faculty of Physics, Lomonosov Moscow State University (Moscow, Russian Federation).
ivan-2002@bk.ru

Elizar N. Koltsov, 3rd year postgraduate student, MIPT, Engineer, Group of Semiconductor and Composite Materials, Federal Research Center for Problems of Chemical Physics and Medicinal Chemistry, RAS (Dolgoprudny, Chernogolovka, Moscow Region, Russian Federation).
elizar.kem@mail.ru

Alena V. Stanchik, Cand. Sci. (Phys.-Math.), Associate Professor, Senior Researcher, Laboratory of Semiconductor Physics, Scientific-Practical Materials Research Centre, National Academy of Sciences of Belarus (Minsk, Republic of Belarus).
https://orcid.org/0000-0001-8222-8030
alena.stanchik@bk.ru

Valery F. Gremenok, D.Sci. (Phys.-Math.), Professor, Head of Laboratory of Semiconductor Physics, Scientific-Practical Materials Research Centre, National Academy of Sciences of Belarus (Minsk, Republic of Belarus).
https://orcid.org/0000-0002-3442-5299
gremenok@physics.by

Received November 8, 2024; accepted after reviewing December 2, 2024; accepted for publication December 4, 2024; published online September 25, 2025.